ELSEVIER International Journal of Coal Geology 34 (1997) 69–88

International Journal of coal geology

Quantitative characterization of coal by means of microfocal X-ray computed microtomography (CMT) and color image analysis (CIA)

Frederik J. Simons [a,1], Frédéric Verhelst [b,*,2], Rudy Swennen [a]

[a] *Fysico-Chemische Geologie, Katholieke Universiteit Leuven, Celestijnenlaan 200C, B-3001 Heverlee, Belgium*

[b] *Department of Civil Engineering, Katholieke Universiteit Leuven, de Croylaan 2, B-3001 Heverlee, Belgium*

Received 24 September 1996; accepted 1 April 1997

Abstract

Microfocal X-ray computed microtomography (CMT) is a novel technique that produces three-dimensional maps of the distribution of the linear attenuation coefficient inside an object. In contrast to the more conventional medical computerized tomography (CT) systems, a microfocal X-ray source is used. This enables a far better spatial resolution. The linear attenuation coefficient or tomodensity is dependent on the physical density and the mineralogy of the object to be imaged, and on the energy of the radiation used. Earlier work by Verhelst et al. (Verhelst, F., David, P., Fermont, W.J.J., Jegers, L., Vervoort, A., 1996. Correlation of 3D-computerized tomographic scans and 2D-color image analysis of Westphalian coal by means of multivariate statistics. Int. J. Coal Geol. 29, 1-21) presented the results of the correlation of the tomodensities obtained from three-dimensional CT scans with two-dimensional data on the composition of a coal sample acquired with color image analysis (CIA), a camera technique. This analysis assumed the linear proportionality of the tomodensity with the real physical bulk density, which is true only for certain energy ranges. In this paper, we use CMT devices for a similar correlation. For sake of comparison, the same core sample was used. First, new CIA data on the surface composition along two profiles were sampled with greater detail (100 μm). These data are subjected to a geostatistical analysis to quantify the spatial dependence between the measurements. Second, CMT tomograms were made, yielding spatial resolutions twice as high as medical CT. A

* Corresponding author.

[1] Present address: Department of Earth, Atmospheric and Planetary Sciences, Massachusetts Institute of Technology, Cambridge, MA 02139, USA. Fax: +1-617-2589697; e-mail: fjsimons@mit.edu

[2] Present address: Center for Technical Geoscience, Delft University of Technology, P.O. Box 5046, NL-2600 GA Delft. E-mail: f.verhelst@ctg.tudelft.nl.

PII S0166-5162(97)00011-6

multivariate correlation was carried out, and two improved (geo)statistical methods are suggested. The different energy range of the microfocal X-ray source compared to medical CT, however, produces some bias in the correlation of the tomodensities with the surface percentages of the constituents. We therefore suggest that the linear attenuation coefficient be treated as a separate unit. No attempt was made to translate the linear attenuation coefficient to the physical bulk density of the different constituents of coal (e.g. macerals). © 1997 Elsevier Science B.V.

Keywords: geostatistics; image analysis; least-squares analysis; macerals; tomography; X-ray analysis

1. Introduction

Previously, Verhelst et al. (1996) correlated three-dimensional tomodensity (or linear attenuation coefficient for X-rays) measurements with two-dimensional compositional data for a linear set of intervals on or near the surface of a coal sample. The tomodensities were obtained with the conventional (medical) computerized tomography (CT) technique, along a profile or *trace* through a coal sample perpendicular to the layering. The percentages of five different constituents of the coal (vitrinite, liptinite, inertinite, pyrite and voids, filled with binder) were acquired on the surface with color image analysis (CIA).

Among the recent developments in CT is the fabrication of systems using *microfocal* X-ray equipment. Computed microtomography (CMT) produces higher-resolution maps of the distribution of the linear attenuation coefficient inside a sample (Sasov, 1987; Jasti et al., 1993; Spanne et al., 1994; Simons, 1996 and references therein). New devices have been made commercially available (Fuhrmann, 1993, 1994, 1995). The performance of microtomography depends on the size of the sample, since the object is placed in a cone beam. The positioning of the sample in the beam will optimize photon counting statistics. The pixel size and highest significant spatial frequency achieved are determined after the measurement. The best way to quantitatively evaluate the reliability of this new technology for the characterization of geologic media, e.g. coal, consists in performing a similar analysis as in Verhelst et al. (1996) on material from the same core sample. In this paper, new surface data on the composition of the same Westphalian A coal treated by Verhelst et al. (1996) are obtained with much smaller sampling intervals than the previous study. This is done to yield smaller pixel sizes suitable for comparison with the enhanced-resolution microfocal CMT measurements. The microtomographic slice through the sample is obtained within only a few tens of microns from the surface.

The real physical composition of the coal material under study has a high intrinsic spatial fluctuation. CIA measurements obtain average compositions of a certain area (called the *support* in geostatistical theory) which is 100×100 μm^2 in this study. It should be noted that this area is larger than the spatial variability of the coal composition. However, this CIA resolution is in turn an order of magnitude better than the resolution of the CMT. This enables us to consider the spatial resolution of the CIA measurements, although not perfect, as the 'reality' to be compared with the CT measurements.

After a brief discussion of the techniques used, the results for both CIA and CMT

will be presented. A multivariate correlation between the compositional measurements and the tomodensities will be performed by means of multiple linear regression analysis. In this paper we present the results obtained with this novel technique and show the potential of correlating CIA with CMT, in comparison with the results of the correlation of CIA with conventional CT as presented in Verhelst et al. (1996). To improve this correlation, we suggest two (geo)statistical methods.

2. Background

2.1. Computerized tomography

The principles of CT and their application to the characterization of geologic media have been discussed elsewhere (Herman, 1980; Wellington and Vinegar, 1987; Swennen et al., 1990; Boespflug et al., 1994; Orsi et al., 1994; Verhelst et al., 1995; Verhelst and Simons, 1997). From a set of projection data taken at different angles, the distribution of the linear attenuation coefficient inside the volume of the sample is reconstructed. X-rays can be considered as waves and as a flow of particles. In the latter description, X-rays are seen as energy quanta. Each X-ray quantum originating from the source can traverse an object with a certain probability. Some quanta do not traverse. This attenuates the beam, which is recorded by the detector as a reduced intensity of radiation. This transmitted intensity is exponentially proportional to the linear attenuation coefficient of the sample following Beer's Law, which describes macroscopically the probabilistic behavior of the energy quanta.

In the energy range of X-ray tubes most frequently used, the linear attenuation coefficient or tomodensity is known to depend predominantly on three different physical interaction processes of radiation with matter. Both the *photoelectric* and the *Rayleigh effect* are influenced by the energy E of the radiation, the effective atomic number Z of the irradiated matter and the bulk density. The *Compton effect* depends only on the energy of the X-ray photons. The linear attenuation coefficient μ (dimension $[L^{-1}]$) can be written as the sum of these three contributions: the first term represents the photoelectric, the second the Compton and the third the Rayleigh effect (Curry et al., 1990)

$$\mu = \frac{1}{2000} \cdot N_A \cdot \rho \left(9.8 \frac{Z^{3.8}}{E^{3.2}} + 0.597 e^{[-0.0028(E-30)]} + 1.25 \frac{Z^{2.5}}{E^{1.9}} \right). \quad (1)$$

N_A is Avogadro's number. For hexagonal carbon with $Z = 6$ and $\rho = 2250$ kg m^{-3} (Klein and Hurlbut, 1993), the linear attenuation coefficient will behave as in Fig. 1. In the energy domain around 100 keV, μ is quasi energy-independent (the almost flat regions of the curve) because the only significant contribution comes from the Compton effect. This independence of energy is important. Compared with the almost monochromatic (single-energy) synchrotron X-ray sources (SXS), conventional X-ray sources

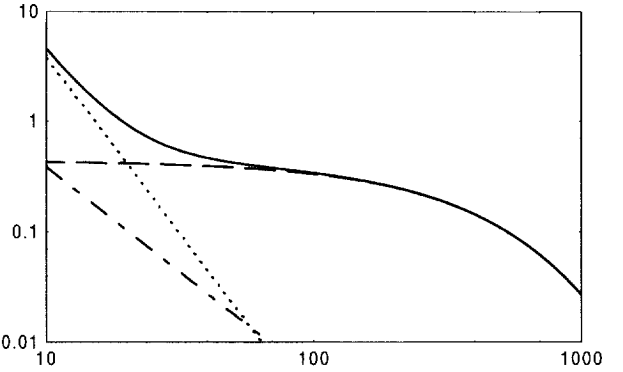

Fig. 1. Energy dependence of the linear attenuation coefficient for hexagonal carbon. *X*-axis: acceleration potential of the source, in keV. *Y*-axis: linear attenuation coefficient in arbitrary units. --- Compton effect. · · · photoelectric effect. – · – Rayleigh effect. ———— sum of the three effects; total linear attenuation.

used for medical purposes (e.g. Verhelst et al., 1995), and the microfocal X-ray sources used in this study, emit a large spectrum of X-ray energies. If μ were energy-dependent within this range, this would cause an undesirable gradual alteration of the energy content of the X-ray beam, since the lower-energy portions of the radiation would be preferentially removed. This process is commonly referred to as *beam hardening*.

Moreover, the Compton effect is independent of the atomic number of the sample, see Eq. (1), causing a linear proportionality of μ with the bulk density of the sample. It is this energy region that is of most interest. Earlier attempts to correlate tomodensity with composition through density by multiple linear regression were carried out in this range.

CMT relies on the enhanced spatial resolution of the individual projections by using a microfocal X-ray tube, thus producing sharper tomographic sections.

2.2. *The microfocal X-ray tube*

Medical CT facilities operate with conventional X-ray tubes. X-rays are generated from the entire target surface since the electrons are poorly focused. Microfocal X-ray tubes (Ely, 1980) are constructed so that electrons are focused before they hit the target (Fig. 2). The X-rays emerge from a tiny area called the *focal spot*. The reduction of the focal spot has several interesting advantages. These will be illustrated for the projection mode of X-radiography. It must be borne in mind that the same considerations pertain to the tomographic mode as well, since a tomogram is reconstructed from a number of projections at different angles.

Two parameters influencing the spatial resolution of the image of an object must be introduced.

The *geometrical* or *penumbral unsharpness* is directly related to the breadth of the source or the size of the focal spot (Fig. 3). If the source, the object and the detector are at a certain distance from each other there will be a part of the detector where X-ray

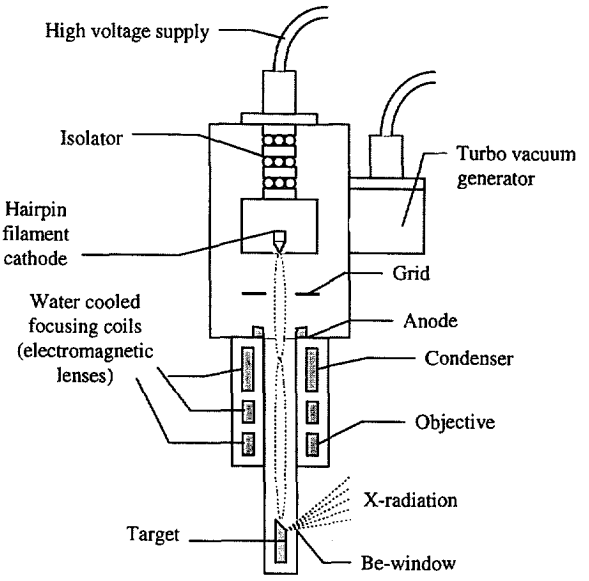

Fig. 2. The microfocal X-ray source.

enery from the entire breadth of the source is detected, attenuated by passing through the object. In Fig. 3 this corresponds to the region from point *d* to *e*. Another region, beyond *f*, records the unattenuated intensity from the entire source. In between these two regions lies the *penumbra*, from *e* to *f*, with an X-ray intensity varying between the maximum (unattenuated) and the minimum (attenuated) intensity. Between this

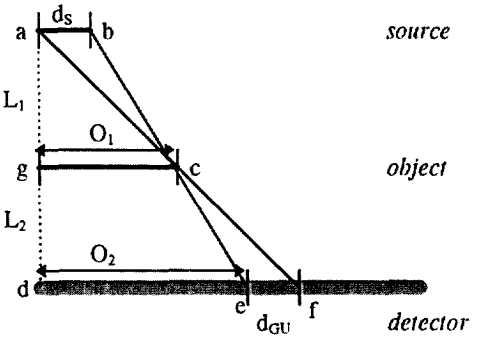

d_S= breadth of the source (focal spot size)

d_{GU}= geometrical unsharpness

Fig. 3. The geometrical unsharpness.

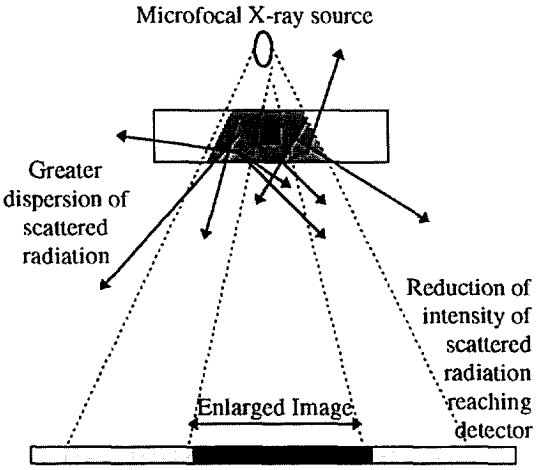

Fig. 4. The reduction of the intrinsic unsharpness (after Ely, 1980).

geometrical unsharpness d_{GU} and the focal spot size d_S, the following relationship holds (Stegemann et al., 1992):

$$d_{GU} = d_S \cdot \frac{L_2}{L_1} \tag{2}$$

The *intrinsic unsharpness* is caused by secondary radiation originating in the object. In the definition of the linear attenuation coefficient, it is assumed that scattered Compton radiation, diffracted Rayleigh radiation or any characteristic X-radiation resulting from the photoelectric absorption process is 'lost' as image-producing radiation. Nevertheless, if these photons reach the detector, they produce noise. This noise can be diminished if the object is placed away from the detector (Fig. 4).

Placing source, object and detector apart enables the image to be enlarged. The *geometrical image magnification M*, can be expressed as (Fig. 3)

$$M = \frac{O_2}{O_1} = \frac{L_1 + L_2}{L_1} = 1 + \frac{L_2}{L_1} \tag{3}$$

and is therefore directly related to the geometrical unsharpness d_{GU} and the focal spot size d_S through the following formula:

$$d_{GU} = d_S \cdot (M - 1) \tag{4}$$

Therefore, the smaller the focal spot size, the more the image can be enlarged with still acceptable geometrical and intrinsic unsharpnesses.

2.3. Color image analysis

Excellent detailed accounts of the principles of CIA and its use in the quantitative characterization of coal have been given elsewhere (David and Fermont, 1993a,b). Here

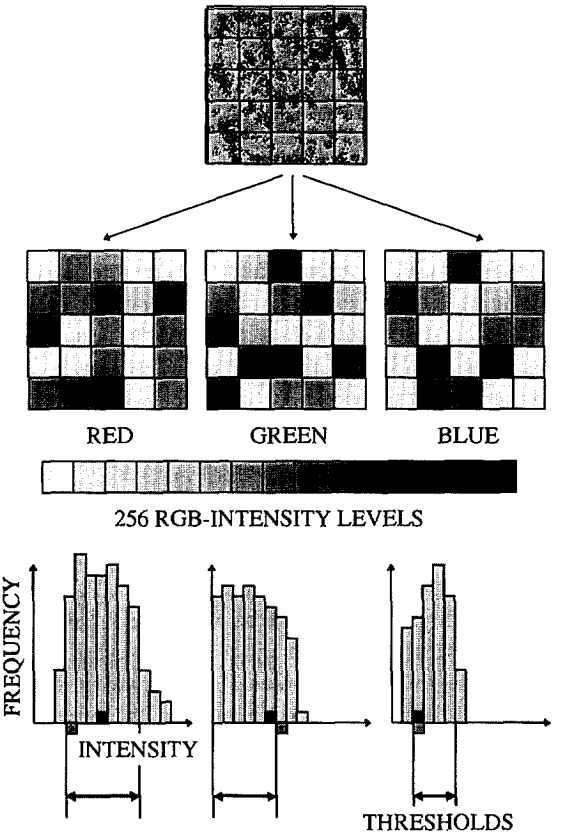

Fig. 5. Schematic representation of CIA (from Simons, 1996).

only a brief summary and a clarifying figure will be given (Fig. 5). CIA allows the quantitative recognition of species on the basis of their color composition. Maceral groups or mineral species are characterized by a range of intensity values for red, green and blue (RGB). The range of intensities considered as 'characteristic' is contained within threshold values that are defined in the calibration phase before each set of measurements. A specific image *pixel* is recognized to belong to a certain mineral group only if its RGB intensities fall within all thresholds defined. A pixel can belong to more groups at the same time if the areas defined by the threshold values in the RGB-space overlap. In such a case, the pixel is assigned to both groups. A pixel that cannot be found to belong to a specific mineral group is left unassigned. Surface percentages of the different components for which thresholds have been defined are calculated as the ratio of the pixels assigned to the particular group divided by the total number of pixels that could be assigned in the image. This illustrates the trade-off between the percentage of the area of the image that can be assigned to a particular group and the accuracy with which this is done. The broader the range between the thresholds, the more easily pixels are recognized and assigned, but the more overlap exists between the groups, resulting

in a poorer species resolution. The calibration consists of adjusting the thresholds until the user is visually satisfied with the result.

2.4. Resampling and Fourier frequency filtering, cross-correlation

Of fundamental importance in the quantitative correlation of signals are the following three considerations.

The signals to be compared must have the same *sampling intervals*. All signals treated by the computer must be represented as discrete samples with a specific sampling interval. To be able to piecewise compare sequences of samples, the sampling intervals should be identical in length (Davis, 1986). This is not a priori the case in the comparison of tomographic with image analysis data. The *resampling* procedure used in this study will be quite straightforward. An average is determined of those sampling intervals of which the central point falls within a new, this time larger, sampling interval.

The two signals must have approximately the same *frequency content*. Following Fourier's theorem, a signal can be written as an integral of sine and cosine terms of continuously varying, spatial, frequency. This integral can be approximated as a finite sum of periodic components with discrete frequencies. The higher (and the more *significant*, that is, showing high amplitudes) the *highest* spatial frequency present in the signal, the more accurately sharp variations in space are described. For two signals with a considerable difference in frequency content, the one with the narrowest frequency content, not being able to follow the sharp changes in the other signal, gives rise to a transition zone at every abrupt variation. In a piece-by-piece comparison of both correlated signals (e.g. by regression analysis), this transition zone causes an extra bias. By adjusting the frequency contents of both signals, the smoothness of the signals will become comparable, and the correlation will be more correct. By means of a fast Fourier transform (FFT) algorithm, the largest significant frequency of all our signals will be determined. This frequency will be called the *cut-off frequency*. The cut-off frequency is related to the maximal spatial resolution. To equalize the frequency contents of both the CMT and the CIA measurements, the amplitudes of the frequencies beyond the cut-off frequency will be set to zero for both signals, and the series will be transformed back into the spatial domain.

A plot of the spatial frequencies and their amplitudes also reveals the possible cyclic behavior of the series. The frequency analysis (not shown here) of the coal in our study showed prominent (depositional?) cycles having periods of about 2.20, 3.08 and 7.70 mm. This property will not be emphasized here, but will be mentioned again later, since the same cycles show up in the experimental variograms.

The relative positioning of the signals will be performed using *cross-correlation* (Davis, 1986). From the tomographic slice through the object, taken as close as possible to the surface, two traces will be obtained that geometrically best match the two surface traces analyzed with CIA. However, both signals may be slightly off-phase. Therefore, the cross-correlation function for both signals will be calculated. Maximizing the cross-correlation function at lag τ corresponds to making both signals overlap maximally. In our study, the cross-correlation between the vitrinite and liptinite contents of

the CIA-signals and the tomodensity signals of the CMT measurements will be maximized by shifting the signals at different relative positions τ. The signals are then kept at the position corresponding to the maximum cross-correlation value, which means that the traces are properly aligned.

A major assumption is that the CIA signal is accurately composed. The stepping from frame to frame has to be performed by hand. Small deviations from the exact interval are inevitable. These fluctuations are not considered crucial, as long as the average error is close to zero, otherwise a cumulative error will be introduced.

2.5. Multiple linear regression analysis

Central to our approach is the assumption that the linear attenuation coefficient or tomodensity μ (expressed in multiples of m^{-1}) varies linearly with the physical density (whose units are kg m^{-3}). This is most likely to be true if the energy spectrum of the X-radiation falls within the flat regions of the curve plotted in Fig. 1. The physical *bulk density* of the coal is of course related to its composition, here expressed as the surface percentage of the constituents. Under the above assumptions, it is reasonable to solve

$$y_i = a + b_1 \cdot x_{1i} + b_2 \cdot x_{2i} + \ldots + b_m \cdot x_{mi} + e_i \quad (5)$$

for the regression coefficients $b_{2 \rightarrow m}$. In this way, the *tomodensity* is considered as the dependent variable y, and the surface percentages of vitrinite (x_1), liptinite (x_2), inertinite (x_3), pyrite (x_4) and voids (x_5), as the independently varying parameters defining y. The term e is an error term that is minimized in a least squares sense. A measure of how well the CIA-surface percentages are successful in predicting the CMT-tomodensity is provided in the *coefficient of multiple determination* R^2. This coefficient can be interpreted in terms of the percentage of the variability of the data that is explained by the regression model versus the total variability of the data, which obviously includes secular variations (random errors or *residuals*) not predicted by the regression line.

Multiple regression analysis is powerful provided some conditions are met (Harnett and Murphy, 1980): (1) As has been stated above: a linear relationship between the variables must be present on physical grounds. (2) A normal distribution of the errors is assumed. The least squares method uses the squared Euclidean length of the error (residual) vector, which inherently weights large errors heavily, and produces bias in the case of longer-tailed distributions (Menke, 1989). Normality is judged from a study of the histograms of the residuals of the analysis (i.e., the difference of the observed versus the predicted values). (3) No correlation is allowed between subsequent observations. The absence or presence of serial correlation can be indicated by the d-value of the *Durbin-Watson test* (Harnett and Murphy, 1980) and quantitatively assessed by a study of the experimental semivariogram of the data (Journel and Huijbregts, 1978). This geostatistical tool is discussed in the following section. Given the method of sampling (along a profile perpendicular to the compositional banding of the coal), the serial dependence is a spatial autocorrelation of the (tomo)density.

The independent variables must be mutually independent. That is, no strong correlations between the independent variables may exist, as the matrix x_{ij} that relates the data

y_i to the model parameters (the independent variables) b_j must not be *ill-conditioned* (Tarantola, 1987). This correlation can be assessed by producing a square *correlation matrix* between the variables. The awareness of this problem is particularly important in the analysis of geological data, since these are generally presented in normalized form, forming a closed sum (this is commonly referred to as the *closure problem*). Therefore, at least one negative correlation between the variables always exists (Whitten, 1993).

2.6. The geostatistical language

Conventional statistics only considers independent observations. This assumption does not hold for geologic parameters, such as the variation of composition or tomodensity perpendicular to the layering of a coal sample. The composition and tomodensity at one point are not independent from those at an adjacent point. Quantification of this *spatial autocorrelation* is the subject of geostatistics. An excellent textbook is available by Journel and Huijbregts (1978). The software used in this paper is GSLIB (Deutsch and Journel, 1992).

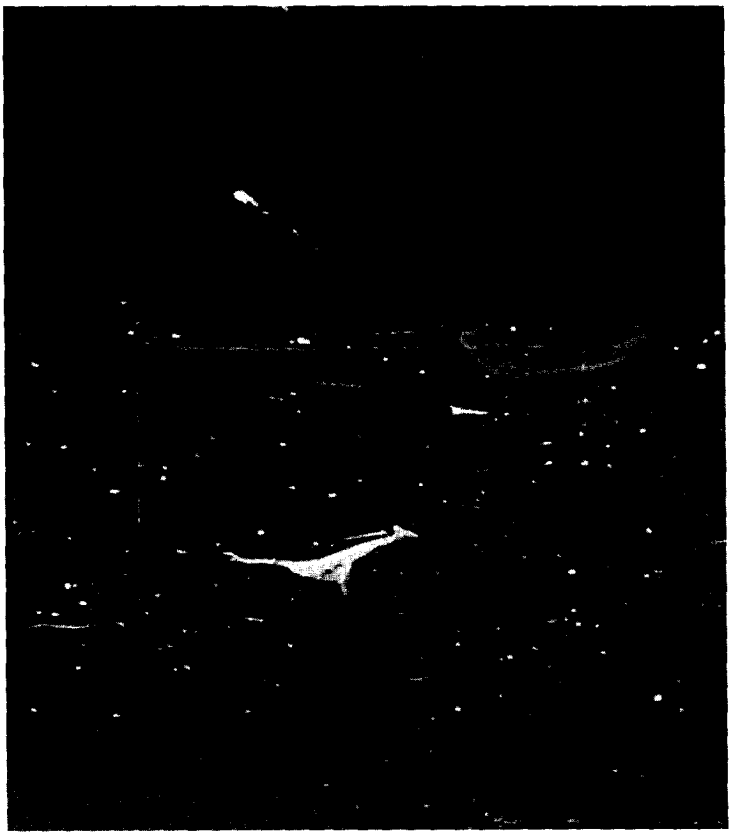

Fig. 6. Photograph of the surface of the coal sample. The frame corresponds to approximately 100 μm.

The experimental semivariogram is a fundamental geostatistical tool. Since the value of a function f at a point x (e.g., the vitrinite content at x, in %) is not independent from the value at $x+h$, a good measure of this autocorrelation in terms of the lag h is the mean of the squared differences (in $\%^2$) between $f(x)$ and $f(x+h)$ over all $n(h)$ possible sets of pairs separated by a distance h. This expression is called the *experimental variogram* $2\gamma^*(h)$

$$2\gamma^*(h) = \frac{1}{n(h)} \cdot \sum_{i=1}^{n(h)} [f(x_i) - f(x_i + h)]^2. \tag{6}$$

The *semi*variogram is given by half this expression. A common theoretical model is the *spherical* semivariogram $\gamma(h)$, which is given by

$$\gamma(h) = c\left(\frac{3h}{2a} - \frac{h^3}{2a^3}\right) \quad \text{for } h \le a \tag{7}$$

$$\gamma(h) = c \quad \text{for } h \ge a \tag{8}$$

The variance of the measurements reappears as the *sill* c of the semivariogram. The distance at which $\gamma(h)$ invariably becomes equal to c is the zone of influence called the *range* a. The value of $\gamma(h)$ may be higher by a term called the *nugget* N. The value of

Fig. 7. CMT-tomogram. The tomodensities are represented by gray scaling. The diameter of the sample is approximately 2 cm.

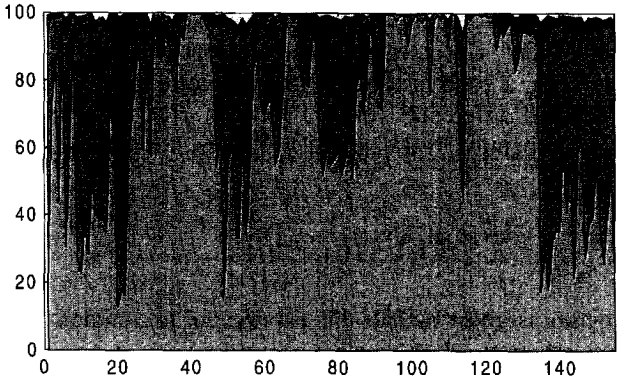

Fig. 8. Cumulative normalized surface percentages of the five constituents sampled along trace 1. Each of the 150 measurements corresponds to a length of 100 μm along the trace. Plotted from the bottom up are vitrinite, liptinite, inertinite, pyrite and binder.

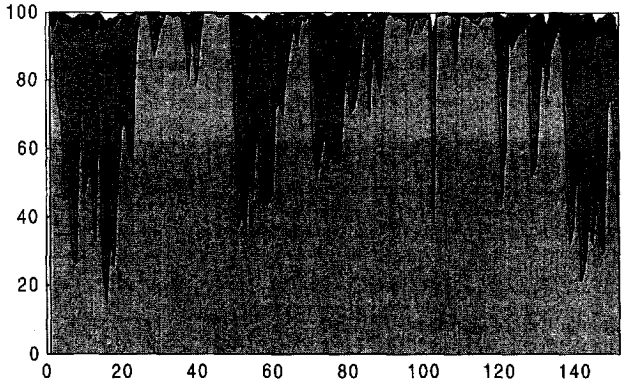

Fig. 9. Cumulative normalized surface percentages of the five constituents sampled along trace 2.

N/c corresponds to the fundamental uncertainty present in the set of observations. This can be understood by means of Fig. 6, where the variability within one frame of the CIA-measurement can be easily distinguished. Due to the support (averaging) of the measurement, that variability cannot be captured by the measurement. One CIA image corresponds to the frame drawn, one CIA result corresponding to the compositional percentages averaged over the frame.

From the above properties it is apparent that periodic (autocorrelated) series have an experimental semivariogram that oscillates with the same frequency. $\gamma(h)$ has minima at distances that correspond to the dominant periods in the signal. This will be made visible by the figures in a later section.

As mentioned before, multiple linear regression analysis requires the serial independence of observations in order to be quantitatively interpretable. In the results presented below, the experimental semivariograms of the data will give an indication of the

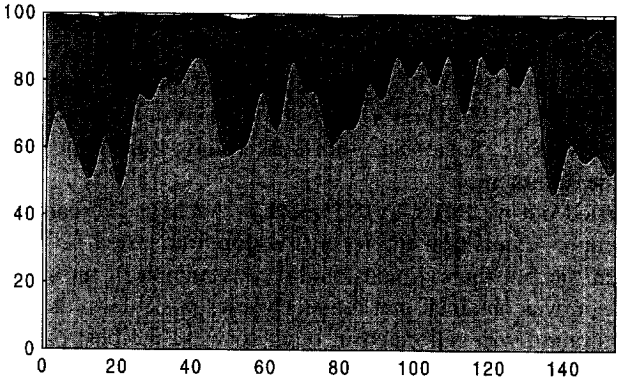

Fig. 10. Filtered normalized surface percentages of trace 1. The highest significant spatial frequency is set to 667 μm, in accordance with the CMT-measurement.

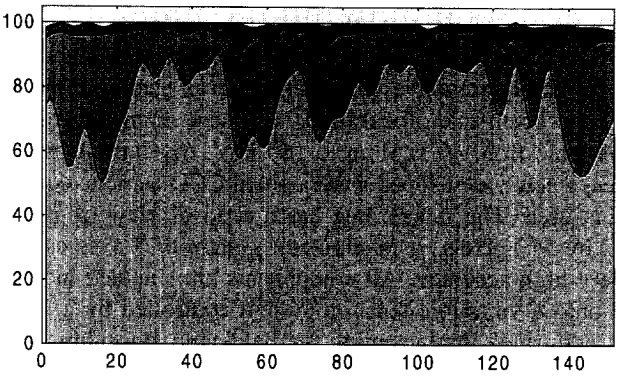

Fig. 11. Filtered normalized surface percentages of trace 2.

presence and the extent of this autocorrelation, by the value of the range a. A suggestion for 'removing' the serial autocorrelation will be given in the discussion.

3. Sample provenance, preparation and measurements

The sample was taken from coal seam 20 (KS 54) of the Peer borehole in Belgium, at a depth of 1108.54–1108.68 m. This seam was previously assigned to the Upper Westphalian A and classified as high volatile A bituminous coal with a vitrinite reflectance of 0.97% R_r (Verhelst et al., 1996). Well Peer was drilled as a pilot well to ascertain the occurrence of methane and the possibilities of coal bed methane extraction (CBM).

On the polished surface of the impregnated sample, two traces, perpendicular to the compositional banding, were followed with CIA, over a length of approximately 1.5 cm.

The two traces were spaced 7.2 mm apart. Each trace was composed of about 150 images of 100×100 μm^2, a significant reduction compared to the 170×300 μm^2 used by Verhelst et al. (1996). The equipment used in this study was the same as described in Helsen et al. (1995) and Verhelst et al. (1996). All settings, i.e. light source, diaphragm, filters, voltage, lenses and threshold values were kept constant throughout calibration and measurements.

CMT was carried out by INTRAVIS GmbH in Aachen, Germany, using an INTOS 160 microtomograph. Acquisition and reconstruction time lasted 120 min each. We used 360 projections in the full three-dimensional reconstruction of the whole sample. From these data, a section was obtained that ran as close as possible to the surface (about 100 μm). The configuration was calibrated in order to yield the best possible images, with the highest signal-to-noise ratio. This required an acceleration voltage of the microfocal X-ray tube of 50 keV. The current through the filament was 100 μA. The image was rotated and the traces were extracted from the section. The pixel size of the slice was 53×53 μm^2.

The resampling procedure described earlier converted both signals to intervals with a length of 100 μm, in accordance with the CIA-measurements.

The INTOS 160 system merits further discussion since a similar system has not been used previously for the quantitative characterization of geologic media. Central is the X-ray source, a cone beam microfocal tube, with spot diameter going down to 5 μm. The voltage is variable from 40 keV up to 160 keV, the current from 100 to 200 μA. For small samples, a newly developed water cooled CCD camera, equipped with a 16 bit A/D converter, is used. The image area has a field of view of 10×10 mm^2 with a resolution of 512 by 512 pixels. A manipulator system of 7 axes can move sample and detectors with very high accuracy. All components are shielded in a leaden box which can be mounted onto a vibration isolation system controlled by a microprocessor. The reconstruction is performed implementing the Feldkamp algorithm, going directly from the projection data to the three-dimensional model without creating two-dimensional slices in the first step, thus incorporating a maximum amount of data. An arbitrary section or *tomogram* can be obtained subsequently.

4. Results

The final tomogram obtained by the CMT-measurement is given in Fig. 7, where the coal constituents clearly exhibit different absorption and scattering behavior for X-rays. The original normalized surface percentages of the maceral groups vitrinite, liptinite, inertinite, the mineral pyrite and the voids, filled with araldite binder, are plotted on top of each other along profile 1 in Fig. 8 and along trace 2 in Fig. 9. Figs. 10 and 11 depict the filtered equivalents of the signals of trace 1 and 2, respectively. FFT-filtering suppressed all frequencies beyond a cut-off which was set to a period of 667 μm, in accordance with the maximum significant spatial frequencies present in the tomodensity signals. This greatly improved the results of Verhelst et al. (1996), who used a cut-off frequency of approximately 1500 μm. Clearly, CMT yields significantly better results as far as the spatial resolution is concerned.

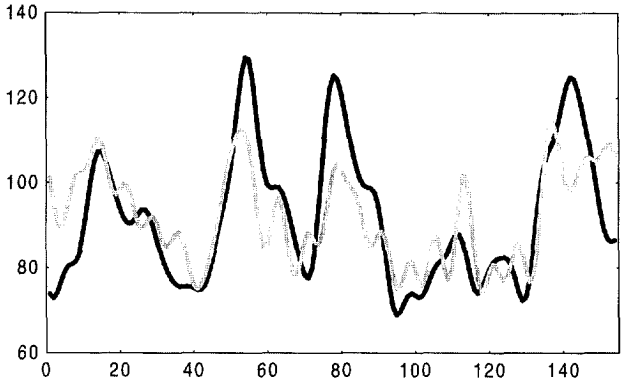

Fig. 12. Results of the multiple regression for trace 1. Gray curve: predicted tomodensity. Black curve: observed tomodensity.

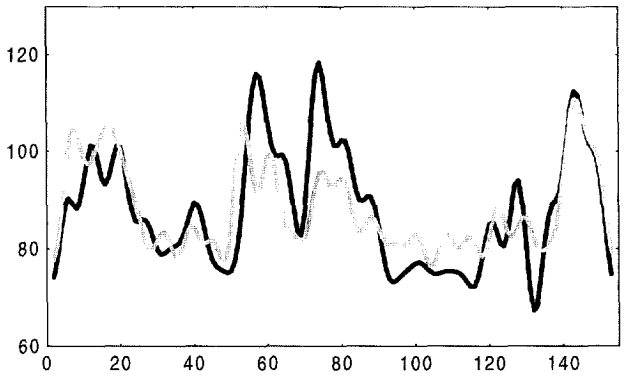

Fig. 13. Results of the multiple regression for trace 2.

In Figs. 12 and 13, the filtered tomodensity signals of trace 1 and 2 are shown, together with the prediction based on the regression equations given by

$$\begin{aligned}\text{TOMODENSITY} = {} & (63.571 \pm 2.683) + (0.707 \pm 0.129) \times (\%\text{LIP}) \\ & + (0.103 \pm 0.370)\text{x}(\%\text{INE}) + (3.941 \pm 3.208) \times (\%\text{PYR}) \\ & + (12.119 \pm 3.841) \times (\%\text{BIN})\end{aligned}$$

for trace 1. The equation for trace 2 becomes

$$\begin{aligned}\text{TOMODENSITY} = {} & (71.473 \pm 1.829) + (0.967 \pm 0.086) \times (\%\text{LIP}) \\ & + (1.226 \pm 0.630) \times (\%\text{INE}) - (1.321 \pm 0.929) \\ & \times (\%\text{PYR}) - (9.092 \pm 2.384) \times (\%\text{BIN}).\end{aligned}$$

where %LIP, %INE, %PYR and %BIN denote the surface percentages of liptinite, inertinite, pyrite and binder, respectively. The multiple coefficient of determination R^2

is 0.481 for trace 1 and 0.539 for trace 2. The uncertainties quoted are standard errors of the regression coefficients. The surface percentage of vitrinite was rejected as an independent variable since its correlation with the liptinite content was too high (-0.933 and -0.990 for the filtered signals of trace 1 and 2). This was to be expected, as mentioned above, since the normalized surface percentages form a closed sum. Vitrinite and liptinite are far more abundant than the three other components. A high vitrinite surface percentage invariably causes a low liptinite percentage. The reverse is also true. Due to the abundance of vitrinite, the closure problem is not so essential for the remaining variables, once we have eliminated vitrinite as an independent variable. We can consider vitrinite as some kind of a background, that fills all the remaining space. The other compositions can be treated as independent variables in a first approximation.

5. Discussion

Visual inspection of the curves warrants the conclusion that there exists a close correlation between the tomodensity of an interval and its surface composition. However, the correlation coefficients are lower than those found in the correlation of CIA with traditional CT measurements as quoted in Verhelst et al. (1996). The medical CT used in the paper by Verhelst and co-workers operated at maximum photon energies of 137 keV. Given the characteristic shape of white X-ray spectra, it was acceptable to infer that the larger part of the energy spectrum fell within the flat part of the curve defined for carbon (Fig. 1). This allowed the assumption of a direct proportionality between the physical bulk density and the linear attenuation coefficient or tomodensity, upon which the multiple linear regression was based. The microfocal X-ray source used in this study operated at maxima of 50 keV. There seems to be an appreciable

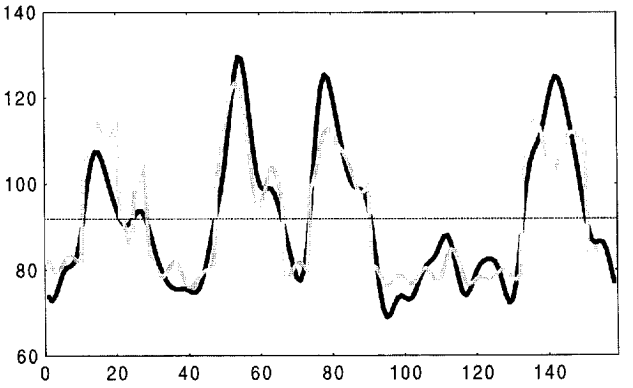

Fig. 14. Results of the breakpoint regression for trace 1. The position of the breakpoint is indicated by the dotted line.

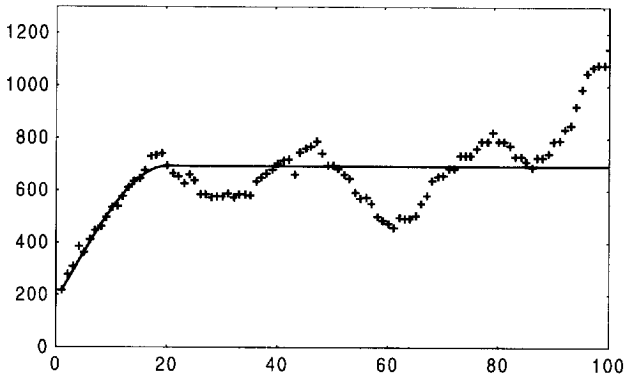

Fig. 15. Experimental semivariogram for the vitrinite surface percentage of trace 1. A spherical model curve was fitted through the data. *X*-axis: distance between pairs in number of observations (each 100 μm). *Y*-axis: semivariogram value in $\%^2$. Range *a*: 19. Sill *c*: 694.32. Nugget *N*: 215.

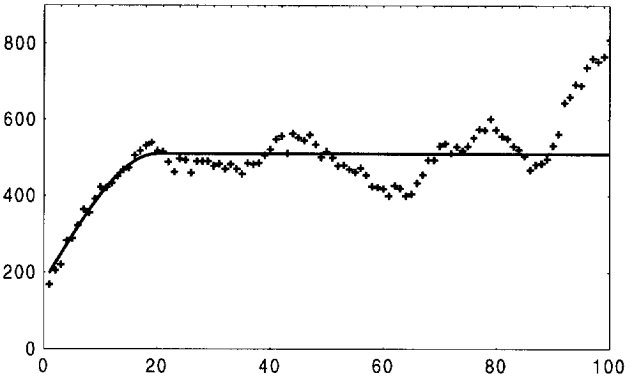

Fig. 16. Experimental semivariogram for the liptinite surface percentage of trace 1. A spherical model curve was fitted through the data. *X*-axis: distance between pairs in number of observations. *Y*-axis: semivariogram value in $\%^2$. Range *a*: 19. Sill *c*: 510. Nugget *N*: 200.

contribution of the photoelectric and Compton effects, which altogether bias the straightforward linear relation with composition.

One way of statistically improving the results is to assure that all variables are normally distributed. This is one of the conditions for multiple linear regression to be quantitatively meaningful. If the dependent variable (the tomodensity) is separated in two subgroups, one above and one below its trace average, and two different regression equations are defined for the two subpopulations, the percentage of variance explained R^2 dramatically increases to 81.587%, which is equivalent to a correlation coefficient R of 0.903. This procedure is known as *piecewise linear regression* or *breakpoint regression*. For trace 1 the predicted versus observed curves following this method are plotted in Fig. 14. Inspection of the normal quantile plots for the two subgroups of

independent variables shows they have a better normal distribution than the group as a whole.

A second, geostatistical, improvement is suggested here. The Durbin–Watson test on the residuals shows that the variables are not independent (the d-value is 0.141 for trace 1 and 0.189 for trace 2, both for about 150 analysed data). The semivariogram not only indicates the presence but also the extent of serial autocorrelation. The experimental semivariograms for the variables vitrinite and liptinite of trace 1 are presented in Figs. 15 and 16. As trace 2 is essentially identical data are not shown. (This was as expected due to the closeness of the two signals (7.2 mm) and the relative lateral continuity of the layering. This supports another major underlying assumption of this study, viz. that the variability in the plane of the layering is negligible. It was therefore reasonable to assume that CIA and CMT measurements, albeit performed at different distances from the surface of the sample, essentially describe the same physical properties.)

Note that, as discussed earlier, the experimental semivariograms oscillate around the sill value according to the cyclicity of the signals. The minimum around 3.00 mm most clearly corresponds to the dominant cycle with the same period that was observed from the frequency analysis.

A theoretical spherical model curve has been fitted through the data. It is obvious that the surface percentages of vitrinite and liptinite show spatial autocorrelation. This is quantified by a geostatistical range of 18 observations or 1800 μm (average range of trace 1 and 2). A possible solution to overcome this problem is making different sets of observations spaced 1800 μm apart, and performing the multiple linear regression analysis on each of these series. The regression coefficients can subsequently be averaged taking into account the reciprocals of their variances, following a procedure described by Hodges and Lehmann (1970) and previously adopted by Verhelst et al. (1996). In this way, the spatial autocorrelation is 'removed' by selecting mutually independent observations. The relative shortness of our data series, however, did not allow for this procedure to be followed, since subseries of only 9 data would be created (9×18 more or less equals the original length of our signals).

Both improvements, however, may be executed on arbitrary data sets which are not sufficiently normally distributed or serially independent for a quantitative appreciation of multiple linear regression to be made.

6. Conclusion

Microfocal X-ray computed microtomography (CMT) is a superior imaging technique. For a sample of approximately $1.5 \times 1.5 \times 1.5$ cm^3, its resolution could be brought down to a pixel size of about 53 μm, with an effective highest spatial frequency corresponding to 667 μm. The tomodensity represents the linear attenuation coefficient for X-rays, which can be interpreted in terms of density and mineralogy. If a direct correlation between the tomodensity and the physical density is sought, however, the peak of the X-ray spectrum should be tuned to the energy region where only Compton scattering occurs. This cannot be done without a priori knowledge of the material to be investigated.

Acknowledgements

The authors wish to thank Dr.-Ing. Gerd Fuhrmann of INTRAVIS GmbH, Kaiserstraße 100, D-52134 Herzogenrath, who provided the tomographic slice through the sample. We are grateful to Dr. Petra David and Dr. Willem J.J. Fermont who helped with the calibration of the color image analysis system and gave the opportunity of using their equipment at the Rijks Geologische Dienst (RGD) Nederland. Mr. Leo Jegers kindly prepared the sample. Dr. Johan van Cleynenbreughel and Ir. Frédéric Maes assisted with the visualization software. This paper sprouted from the principal author's Master's thesis. Many more people contributed to the realization of that work, to whom FJS expresses his gratitude. Dr. Thomas Orsi, Dr. R.R. Dutcher and an anonymous reviewer are thanked for a critical reading of the manuscript.

Addintional explanation and figures may be found at: http://wwwak.tn.tudelft.nl/~fre/KULeuven/ct_cia.html

References

Boespflug, X., Long, B.F.N., Occhietti, S., 1994. CAT-scan in marine stratigraphy: A quantitative approach. Mar. Geol. 122, 281–301.

Curry, T.S., Dowdey, J.E., Murry, R.C., 1990. Christensen's Physics of Diagnostic Radiology, 4th ed. Lea and Febiger, Philadelphia, 522 pp.

David, P., Fermont, W.J.J., 1993a. Application of color image analysis in coal petrology. Org. Geochem. 20 (6), 747–758.

David, P., Fermont, W.J.J., 1993b. Determination of coal maceral composition by means of color image analysis. Fuel Proc. Technol. 36, 9–15.

Davis, J.C., 1986. Statistics and Data Analysis in Geology, 2nd ed. Wiley, New York, 646 pp.

Deutsch, C.V., Journel, A.G., 1992. GSLIB, Geostatistical Software Library and User's Guide. Oxford U.P., Oxford, 340 pp.

Ely, R.V., 1980. Microfocal Radiography. Academic Press, London, 295 pp.

Fuhrmann, G., 1993. Entwicklung eines Mikrotomographiesystems als Zusatz für Rasterelektronenmikroskope. Doctoral thesis, Forschungszentrum Jülich, Jülich, 119 pp.

Fuhrmann, G., 1994. High Resolution X-ray Detector with Scintillating Fiber Optic. 3rd Int. Symp. on Ind. Computertomography, Berlin, 9–11 June 1994.

Fuhrmann, G., 1995. Microtomography: nondestructive quantitative image analysis for soil and rock samples, In: Mann, U., Poelchau, H.S., Steingrobe, B. (Eds.), Information Processing and Modeling in Geology. Aachen Sedimentology Group, 10th Annu. Meeting, pp. 16–20.

Harnett, D.L., Murphy, J.L., 1980. Introductory Statistical Analysis. Addison-Wesley Publishing Company, Reading, 656 pp.

Helsen, S., David, P., Fermont, W.J.J., 1995. Calibration of conodont alteration using color image analysis. J. Geol. 103, 257–267.

Herman, G.T., 1980. Image reconstruction from projections. The fundamentals of Computerized Tomography. Academic Press, New York, 316 pp.

Hodges, J.L., Lehmann, E.L., 1970. Basic concepts of probability and statistics. Holden-Day, San Francisco, 441 pp.

Jasti, J.K., Jesion, G., Feldkamp, L., 1993. Microscopic imaging of porous media with X-ray Computer Tomography. Soc. Petrol. Eng. Form. Eval., Sept. 1993, pp. 189–193.

Journel, A.G., Huijbregts, C.J., 1978. Mining geostatistics. Academic Press, London, 600 pp.

Klein, C., Hurlbut, C.S., 1993. Manual of Mineralogy, 21st ed. Wiley, New York, 681 pp.

Menke, W., 1989. Geophysical Data Analysis: Discrete Inverse Theory, Rev. ed. Academic Press, San Diego, 289 pp.

Orsi, T.H., Edwards, C.M., Anderson, A.L., 1994. X-ray computed tomography: a nondestructive method for quantitative analysis of sediment cores. J. Sediment. Res. A 64, 690–693.

Sasov, A.Y., 1987. Microtomography. I. Methods and equipment. II. Examples of applications. J. Microsc. 147, 169–192.

Simons, F.J., 1996. Quantitative Characterization of Coal by Means of Microfocal X-ray Computed Microtomography (CMT) and Color Image Analysis (CIA). M.Sc. thesis. Katholieke Universiteit Leuven, Leuven, 170 pp. (in Dutch, with English abstract).

Spanne, P., Thovert, J.F., Jacquin, C.J., Lindquist, W.B., Jones, K.W., Adler, P.M., 1994. Synchrotron computed microtomography of porous media: Topology and transports. Phys. Rev. Lett. 73, 2001–2004.

Stegemann, D., Schmidbauer, J., Reimche, W., Camerini, C., Sperandio, A., Fontolan, M.R., Moura Neto, R.J., 1992. Microfocus-Radiography, uses and perspectives. In: Hallai C., Kulcsar, P. (Eds.), Non-Destr. Test. 92, 674–678.

Swennen, R., Poot, B., Marchal, G., 1990. Computerized Tomography as a tool in reservoir characterization. Zentralbl. Geol. Palaeont. Teil I 8, 1105–1124.

Tarantola, A., 1987. Inverse problem theory. Methods for data fitting and model parameter estimation. Elsevier, Amsterdam, 613 pp.

Verhelst, F., Vervoort, A., De Bosscher, Ph., Marchal, G., 1995. X-ray Computerized Tomography: determination of heterogeneities in rock samples. In: Fujii, T. (Ed.), Proc. of the 8th Int. Cong. on Rock Mech. Int. Soc. for Rock Mech., Tokyo, pp. 105–108.

Verhelst, F., David, P., Fermont, W.J.J., Jegers, L., Vervoort, A., 1996. Correlation of 3D-computerized tomographic scans and 2D-color image analysis of Westphalian coal by means of multivariate statistics. Int. J. Coal Geol. 29, 1–21.

Verhelst, F., Simons, F.J., 1997. X-ray Computerized Tomography prior and posterior to Brazilian tensile testing. in prep.

Wellington, S.L. and Vinegar, H.J., 1987. X-ray computerized tomography. J. Petrol. Technol., 885-898.

Whitten, E.H.T., 1993. A solution to the percentage-data problem in petrology. In: Davis, J.C., Herzfeld, U.C., (Eds.), Computers in Geology: 25 years of progress. Int. Assoc. for Math. Geol. Studies in Math. Geol. No. 5, Oxford U.P., New York, 298 pp.